

Supplement of Atmos. Meas. Tech., 13, 2457–2472, 2020
<https://doi.org/10.5194/amt-13-2457-2020-supplement>
© Author(s) 2020. This work is distributed under
the Creative Commons Attribution 4.0 License.



Supplement of

Characterization of anthropogenic organic aerosols by TOF-ACSM with the new capture vaporizer

Yan Zheng et al.

Correspondence to: Qi Chen (qichenpku@pku.edu.cn)

The copyright of individual parts of the supplement might differ from the CC BY 4.0 License.

Section A. Aromatic SOA generated by the OFR experiments

Two types of aromatic SOA are generated in a commercially manufactured oxidation flow reactor (OFR) from Aerodyne Inc. The reactor is an aluminum cylinder with an internal volume of 13.3 L. With a total flow of ~ 7.8 L min^{-1} , the average residence time is about 102 s. In this study, only 254 nm photons are available in the reactor. The ozone with a concentration of 5 ppm are generated outside and continuously introduced into the reactor. The water vapor is carried by the synthetic air through ultrapure water and used to generate OH radicals in the reactor by the reactions of $\text{O}_3 \xrightarrow{254 \text{ nm } h\nu} \text{O}_2 + \text{O}(^1\text{D})$ and $\text{O}(^1\text{D}) + \text{H}_2\text{O} \rightarrow 2\text{OH}$. The RH and temperature are monitored in real time, which are about 22% and 23 °C. The absolute water vapor content is 0.38% under this condition. The NO are produced by injecting N_2O with a volume ratio of $\sim 2\%$ into the reactor, following the reaction of $\text{O}(^1\text{D}) + \text{N}_2\text{O} \rightarrow 2\text{NO}$. Two typical aromatic precursors, toluene (40 ppbv) and benzene (100 ppbv), are continuously introduced into the OFR to produce SOA by the photochemical reactions. These two types of SOA are then measured by the CV ToF-ACSM. The photon flux of the light is determined based on the calibration experiments with SO_2 . The following parameters are used in the PAMchem model to estimate the OH exposure and the NO:HO₂ ratios, including precursor concentrations, 5 ppmv ozone, 0.38% water vapor, 2% N_2O , 1.5×10^{14} photons $\text{cm}^{-2} \text{sec}^{-1}$ at 2V lamp voltage for 254 nm).

15 Section B. PMF analysis

Determination of the PMF solution

PMF analysis was conducted on the organic mass spectra by using the Igor PMF evaluation tool (PET, version 3.00B) (Paatero and Tapper, 1994; Ulbrich et al., 2009). For the TOF-ACSM, the unit-mass-resolution (UMR) data between m/z 20 and 200 are used in the PMF analysis. For the LTOF-AMS, both UMR and high-resolution (HR, a mass resolution of >5000) data are used. The UMR PMF used the spectra between m/z 20 and 200, while the HR PMF analysis used the spectra between m/z 20 and 130, respectively. Eight to nine factors were tested in the PMF runs with various seed (0-50) and rotational parameter (f_{peak}) values. Unless otherwise noted, results are presented for both the model error and the seed number of zero. PMF produces a fit to the data, which is called a solution. The solution contains a set of factors and concentrations. For the CV UMR data in this study, a 6-factor solution was determined. Seven or more factor solutions for the CV UMR data lead to clear splitting of the factors and therefore are not considered. The six statistical OA factors identified by the CV UMR PMF analysis are labeled as more-oxidized oxygenated OA (MO-OOA), less-oxidized oxygenated OA (LO-OOA), hydrocarbon-like OA (HOA), and the OA factors possibly related to cooking (COA), biomass burning (BBOA), and coal combustion (CCOA). The 6-factor solution is also consistent with the previous studies for winter Beijing. For the SV AMS data, a 7-factor solution was determined from both HR and UMR PMF analysis. Except the four primary OA factors and MO-OOA, two LO-OOA factors were identified. For the purpose of comparison, we combined LO-OOA1 and LO-OOA2 to be LO-OOA to compare with the 6-factor solution from the CV UMR data and previous findings in literature. The uncertainties of PMF calculation were examined by the bootstrap analysis. Detailed information about the PMF analysis and the reasons of factor-solution choices are provided in Tables S6-S12 and Figs. S16-20.

35 The 7-factor PMF solution for SV AMS (HR and UMR)

As for the SV HR data, factor numbers from 1 to 8 were run in the model. The model was also run with 6-factor and 7-factor at different f_{peak} values (i.e., -1 to 1, stepped by 0.2) and seed values of 0-50. The 6-factor solutions at f_{peak} of -1, -0.8, -0.6 were not converged. The converged 6-factor solutions at different f_{peak} values are similar with Q/Q_{exp} of 2.908 ± 0.002 . With this choice of solution, HOA and CCOA are mixed and two LO-OOA factors present. The 7-factor solutions were not converged at f_{peak} of -1, -0.8, 1. The converged solutions are similar with Q/Q_{exp} of 2.650 ± 0.001 . The PMF solutions at different seed values show minor differences. We combined the two LO-OOA factors into one LO-OOA factor for the purpose of comparisons. Correlation coefficients (Pearson's R) of the six OA factors with tracers are listed in Table S7. MO-OOA is best correlated with inorganic salts and is the only factor which is highly correlated with RH. LO-OOA does not show distinctively strong correlation with any external tracers. COA is well correlated with two marker ion for cooking activities ($\text{C}_5\text{H}_8\text{O}^+$ and $\text{C}_6\text{H}_{10}\text{O}^+$), distinguishing the COA factor from other factors. BBOA is best correlated with the tracer ion ($\text{C}_2\text{H}_4\text{O}_2^+$) of biomass burning. HOA shows good correlations with benzene, toluene, and NOx. CCOA is best correlated with naphthalene and particle-phase PAH.

As for the SV UMR data, factor numbers from 1 to 9 were run in the model. The model was also run with 7-factor at different f_{peak} values (i.e., -1 to 1, stepped by 0.2) and seed values of 0-50. Only f_{peak} at -0.8, -0.6, -0.4, -0.2, and 0 were converged. The PMF results at f_{peak} of -0.8 and 0 were compared in Fig. S19. The differences in the factor mass spectra and loading time series are small. The PMF solutions at different seed values showed minor discrepancies as well. The 7-factor solution of the UMR data are similar to that of the HR data. Similar to the HR data, we combined the two LO-OOA factors into one LO-OOA factor. Correlation coefficients (Pearson's R) of the six OA factors with tracers are listed in Table S9. Unlike LO-OOA from the HR results which only moderately correlates with all the external tracers ($R < 0.7$), LO-OOA from the UMR results is better correlated with $\text{C}_5\text{H}_8\text{O}^+$, $\text{C}_2\text{H}_4\text{O}_2^+$, and acetaldehyde, suggesting that LO-OOA might not be so well separated in the UMR data as in the HR data. Besides, the diurnal pattern of the UMR HOA indicates a certain degree of mixing with COA (Fig. S12). Overall, the HR and UMR PMF results for the SV-AMS are consistent (Fig. S14). Factor concentrations are temporally well correlated. The difference in factor loadings are generally below 35%.

60 **The 6-factor PMF solution for CV-ACSM (UMR)**

As for the CV UMR data, factor numbers from 1 to 8 were run in the model. The model was also run with 6-factor at different f_{peak} values (i.e., -1 to 1, stepped by 0.2) and seed values of 0-50. As indicated in Fig. S18, the PMF solutions at f_{peak} other than 0 were not converged. The solutions at most of the selected seed numbers were similar to the solution at seed of zero. For the four 6-factor solutions at seed 4, 37, 41, 46, the time-series of the PMF factors are similar. The HOA factor is mixed with the CCOA factor. The LO-OOA factor is somewhat mixed with the MO-OOA factor (Fig. S20). Correlation coefficients (Pearson's R) of the six OA factors with tracers are listed in Table S11. MO-OOA is best correlated with inorganic salts and is the only factor which is highly correlated with RH. LO-OOA does not show distinctively strong correlation with any external tracers. COA is well correlated with two marker ion for cooking activities ($\text{C}_5\text{H}_8\text{O}^+$ and $\text{C}_6\text{H}_{10}\text{O}^+$), distinguishing the COA factor from other factors. BBOA is best correlated with the tracer ion ($\text{C}_2\text{H}_4\text{O}_2^+$) of biomass burning. HOA shows good correlation with benzene, toluene, and NOx. CCOA is best correlated with naphthalene and PAHs.

References

- Decarlo, P. F., Kimmel, J. R., Trimborn, A., Northway, M. J., Jayne, J. T., Aiken, A. C., Gonin, M., Fuhrer, K., Horvath, T., and Docherty, K. S.: Field-deployable, high-resolution, time-of-flight aerosol mass spectrometer, *Anal. Chem.*, 78, 8281-8289, 2006.
- Fröhlich, R., Cubison, M. J., Slowik, J. G., Bukowiecki, N., Prévôt, A. S. H., Baltensperger, U., Schneider, J., Kimmel, J. R., Gonin, M., and Rohner, U.: The ToF-ACSM: a portable aerosol chemical speciation monitor with TOFMS detection, *Atmos. Meas. Tech.*, 6, 3225-3241, 2013.
- Hu, W. W., Hu, M., Hu, W., Jimenez, J. L., Yuan, B., Chen, W. T., Wang, M., Wu, Y. S., Chen, C., Wang, Z. B., Peng, J. F., Zeng, L. M., and Shao, M.: Chemical composition, sources, and aging process of submicron aerosols in Beijing: contrast between summer and winter, *J. Geophys. Res.*, 121, 1955-1977, 10.1002/2015jd024020, 2016.
- Hu, W. W., Campuzano-Jost, P., Day, D. A., Croteau, P., Canagaratna, M. R., Jayne, J. T., Worsnop, D. R., and Jimenez, J. L.: Evaluation of the new capture vaporizer for aerosol mass spectrometers (AMS) through field studies of inorganic species, *Aerosol Sci. Technol.*, 51, 735-754, 10.1080/02786826.2017.1296104, 2017.
- Middlebrook, A. M., Bahreini, R., Jimenez, J. L., and Canagaratna, M. R.: Evaluation of composition-dependent collection efficiencies for the Aerodyne aerosol mass spectrometer using field data, *Aerosol Sci. Technol.*, 46, 258-271, 2012.
- Onasch, T. B., Trimborn, A., Fortner, E. C., Jayne, J. T., Kok, G. L., Williams, L. R., Davidovits, P., and Worsnop, D. R.: Soot particle aerosol mass spectrometer: development, validation, and initial application, *Aerosol Sci. Technol.*, 46, 804-817, 10.1080/02786826.2012.663948, 2012.
- Paatero, P., and Tapper, U.: Positive matrix factorization - A nonnegative factor model with optimal utilization of error-estimates of data values, *Environmetrics*, 5, 111-126, 10.1002/env.3170050203, 1994.
- Ulbrich, I. M., Canagaratna, M. R., Zhang, Q., Worsnop, D. R., and Jimenez, J. L.: Interpretation of organic components from positive matrix factorization of aerosol mass spectrometric data, *Atmos. Chem. Phys.*, 9, 2891-2918, 10.5194/acp-9-2891-2009, 2009.
- Xu, W., Croteau, P., Williams, L., Canagaratna, M., Onasch, T., Cross, E., Zhang, X., Robinson, W., Worsnop, D., and Jayne, J.: Laboratory characterization of an aerosol chemical speciation monitor with PM_{2.5} measurement capability, *Aerosol Sci. Technol.*, 51, 69-83, 10.1080/02786826.2016.1241859, 2017.

Table S1. Instrument details for the ToF-ACSM and the LToF-AMS. The RIE values of nitrate, sulfate, and ammonium for the ToF-ACSM were calibrated by size-selected pure ammonium nitrate and ammonium sulfate particles.

Parameter	ToF-ACSM	LToF-AMS
Vaporizer	CV	SV
RIE _{nitrate}	1.05 ^a	1.1 ^b
RIE _{OA}	1.4 ^b	1.4 ^b
RIE _{chloride}	1.3 ^b	1.3 ^b
RIE _{sulfate}	1.6 ^c	1.2 ^b
RIE _{ammonium}	3.7 ^c	4.0 ^b
CE	1	0.5
Fragment Table	Updated Frag_SO ₃	Default
Mass resolution	~350	~5000 (V mode)

^areported by Xu et al (2017);

^bdefault;

^ccalibrated herein.

Table S2. Detection limits for the ToF-ACSM and the LToF-AMS herein compared to the reference values. All values are scaled by $\sqrt{t_{\text{measure}}/t_{60\text{s}}}$ to refer to 1-min detection limits.

Detection limit (ng m ⁻³)	ToF-ACSM		L-ToF-AMS	HR-ToF-AMS	
	This study	(Fröhlich et al., 2013)	This study	V-mode (Decarlo et al., 2006)	W-mode (Decarlo et al., 2006)
OA	351.8	198	45	22	360
Sulfate	33.6	18	8.1	5.2	110
Nitrate	41.8	21	4.2	2.9	32
Ammonium	470.3	182	2.3	38	150
Chloride	31.4	11	4.6	12	53

Table S3. Updated fragmentation table for the CV ToF-ACSM compared to other entries in the literature. Users are recommended to obtain their own frag_SO₃ by calibrating their instrument with pure (NH₄)₂SO₄ particles.

<i>m/z</i> / ion	Frag_sulfate	Frag_SO ₃			
		SV (default)	CV ToF-ACSM (this study)	CV HR-ToF-AMS (Hu et al., 2017)	CV Q-AMS (Xu et al., 2017)*
18 / H ₂ O ⁺	Frag_SO ₃ [18]	0.67*frag_SO ₃ [64], 0.67*frag_SO ₃ [48]	0.45*frag_SO ₃ [64], 0.45*frag_SO ₃ [48]	0.56*frag_SO ₃ [64], 0.56*frag_SO ₃ [48]	0.938*frag_SO ₃ [64], 0.938*frag_SO ₃ [48]
32 / S ⁺	Frag_SO ₃ [18], Frag_H ₂ SO ₄ [32]	0.21*frag_SO ₃ [64], 0.21*frag_SO ₃ [48]	0.14*frag_SO ₃ [64], 0.14*frag_SO ₃ [48]	0.05*frag_SO ₃ [64], 0.05*frag_SO ₃ [48]	0.105*frag_SO ₃ [64], 0.105*frag_SO ₃ [48]

*Note that Xu et al. (2017) also modified frag_H₂SO₄ from 0.068*frag_H₂SO₄[81], 0.068*frag_H₂SO₄[98] to 0.034*frag_H₂SO₄[81], 0.034*frag_H₂SO₄[98] except frag_SO₃.

Table S4. Values of f_{60} and f_{55}/f_{57} from different anthropogenic sources.

Anthropogenic Sources	Values of f_{60} (%)	Values of f_{55}/f_{57}
WSOA from Biomass Burning (Rice Straw)	0.482	2.69
WSOA from Biomass Burning (Corn Straw)	0.232	2.82
WSOA from Biomass Burning (Wheat Straw)	0.186	3.24
Cooking Exhaust	0.072	4.05
Combustion Exhaust of Bituminous Coal	0.043	0.86
Combustion Exhaust of Anthracite	0.198	2.94
Combustion Exhaust of Lignite	0.033	1.21
Vehicle Exhaust	0.038	1.28
SOA: Photooxidation of Toluene	0.099	3.10
SOA: Photooxidation of Benzene	0.263	2.91

Table S5. Comparisons of the elemental ratios and the OM-to-OC ratios between our study (SV HR analysis) and the previous study.

OA factors	OM/OC		O/C		H/C		N/C	
	This study	Hu et al. (2016)						
CCOA	1.39	1.35	0.17	0.16	1.60	1.56	0.026	0.06
BBOA	1.66	1.45	0.33	0.22	1.88	1.55	0.048	0.021
COA	1.36	1.35	0.14	0.14	1.84	1.75	0.020	0.0049
HOA	1.32	1.38	0.10	0.15	1.94	1.75	0.025	0.027
LO-OOA	1.83	1.81	0.50	0.47	1.55	1.65	0.032	0.039
MO-OOA	2.23	1.91	0.78	0.58	1.74	1.47	0.040	0.014

Table S6. Detailed descriptions of the PMF solutions (SV-AMS, HR data).

Factor Number	Fpeak	Seed	Q/Q_{exp}	Solution Description
1	0	0	10.81	Too few factors and large residuals
2	0	0	6.83	Too few factors. Q/Q_{exp} substantially decreases (37% of the maximum Q) but there still exist large residuals at time periods and key m/z . One of the two factors is POA-like while another is OOA-like.
3	0	0	4.49	Too few factors. Q/Q_{exp} substantially decreases (22% of the maximum Q) but there still exist large residuals at time periods and key m/z . Two factors are POA-like and one is OOA-like.
4	0	0	3.75	Q/Q_{exp} still decreases fast (7% of the maximum Q). The four factors are two POA-like factors and two OOA-like factors (LO-OOA and MO-OOA). More factors are needed.
5	0	0	3.26	Q/Q_{exp} decreases by 5% of the maximum Q . The two POA-like factors remain unchanged while a new OOA factor is separated apart from LO-OOA and MO-OOA. This OOA factor demonstrate similar temporal variation ($R=0.67$), mass spectra ($R=0.77$), and elemental ratio (the O/C ratio of one factor is 0.132 and another is 0.139) as the LO-OOA factor solved in the previous 4-factor solution. This could be factor splitting. However, the POA factors are still not well separated, e.g. HOA mixed with CCOA and BBOA. Therefore, more factors are needed.
6	0	0	2.91	Q/Q_{exp} decreases by 3% of the maximum Q . The three OOA factors remain unchanged while a new POA factor is separated. The three POA factors are BBOA-like, COA-like, and HOA-CCOA mixed. Therefore, more factors are needed.
7	0	0	2.65	Optimum choices for PMF factors (MO-OOA, LO-OOA1, LO-OOA2, HOA, COA, CCOA and BBOA). Time series and diurnal variations of PMF factors are consistent with the external tracers. Besides, the spectra of seven factors are consistent with the source spectra of SV obtained from the AMS spectra database.
8	0	0	2.43	Q/Q_{exp} decreases little (<2% of the maximum Q). Factors split, e.g., BBOA.

Table S7. Correlation coefficients (Pearson's R) of the six OA factors determined from the SV HR data with external tracers, including gas and aerosol species, meteorology parameters. The top-five values of each OA factor are bold.

	MO-OOA	LO-OOA*	COA	BBOA	HOA	CCOA
Acetaldehyde	0.72	0.69	0.67	0.87	0.86	0.58
Acetone	0.75	0.66	0.57	0.84	0.81	0.58
Acetonitrile	0.56	0.50	0.45	0.73	0.75	0.61
Ammonium	0.96	0.55	0.45	0.63	0.61	0.34
Benzene	0.71	0.67	0.58	0.89	0.87	0.70
BP	0.04	-0.16	-0.10	-0.14	-0.09	-0.08
C ₂ H ₄ O ₂ ⁺	0.61	0.69	0.70	0.95	0.89	0.74
C ₃ H ₈ O ⁺	0.55	0.68	0.94	0.78	0.82	0.45
C ₆ H ₁₀ O ⁺	0.44	0.64	0.97	0.72	0.79	0.41
Chloride	0.81	0.66	0.49	0.79	0.78	0.62
CO	0.76	0.55	0.54	0.86	0.82	0.62
Naphthalene	0.59	0.54	0.47	0.89	0.86	0.83
Nitrate	0.93	0.59	0.48	0.63	0.59	0.33
NO	0.51	0.26	0.43	0.75	0.82	0.61
NO ₂	0.52	0.63	0.65	0.79	0.80	0.59
NO _x	0.56	0.41	0.54	0.82	0.87	0.65
O ₃	-0.39	-0.46	-0.52	-0.68	-0.69	-0.60
Ox	0.56	0.68	0.63	0.66	0.68	0.33
PAH	0.15	0.49	0.45	0.63	0.77	0.78
RH	0.81	0.26	0.26	0.56	0.56	0.41
SO ₂	0.15	0.58	0.36	0.60	0.51	0.57
Sulfate	0.98	0.34	0.34	0.47	0.49	0.20
Temp	-0.21	-0.06	-0.05	-0.26	-0.25	-0.34
Toluene	0.64	0.66	0.67	0.87	0.91	0.65
WS	-0.30	-0.39	-0.42	-0.51	-0.50	-0.39

*We combined LO-OOA1 and LO-OOA2 into one factor LO-OOA.

Table S8. Detailed descriptions of the PMF solutions (SV-AMS, UMR data).

Factor Number	Fpeak	Seed	Q/Q_{exp}	Solution Description
1	0	0	17.74	Too few factors and large residuals
2	0	0	-	Too few factors and not converged.
3	0	0	5.38	Too few factors. Q/Q_{exp} substantially decreases (70% of the maximum Q). Two factors are POA-like and one is OOA-like. The three factors are not well separated, e.g. evident signal at m/z 60 exists in all the factors.
4	0	0	4.22	Q/Q_{exp} decreases by 7% of the maximum Q . An extra OOA factor is separated. The four factors are two POA-like factors and two OOA-like factors. Ions at m/z 60 are separated into three of the factors. More factors are needed.
5	0	0	3.46	Q/Q_{exp} decreases by 4% of the maximum Q . The two OOA-like factors remain unchanged while a new POA factor is separated apart. The three POA-like factors are CCOA-like, HOA-like, and COA-like. These factors are not well separated, e.g. ions at m/z 60 are separated into three of the factors. More factors are needed.
6	0	0	3.08	Q/Q_{exp} decreases by 2% of the maximum Q . The two OOA factors remain unchanged while a new POA factor is separated. The four POA factors are BBOA, COA, HOA, and CCOA.
7	0	0	2.71	Optimum choices for PMF factors. An extra OOA factor is separated out. Similar to HR results, seven factors (MO-OOA, LO-OOA1, LO-OOA2, HOA, COA, CCOA and BBOA) are separated. Time series and diurnal variations of PMF factors are consistent with the external tracers. Besides, the spectra of seven factors are consistent with the source spectra of SV obtained from the AMS spectra database. These factors are well correlated with the HR factors (Fig. S9).
8	0	0	2.35	Factors split, e.g., BBOA.
9	0	0	2.43	Factors split, e.g., BBOA, CCOA.

Table S9. Correlation coefficients (Pearson's *R*) of the six OA factors determined from the SV UMR data with external tracers. The top-five values of each OA factor are bold.

	MO-OOA	LO-OOA*	COA	BBOA	HOA	CCOA
Acetaldehyde	0.78	0.78	0.82	0.89	0.90	0.56
Acetone	0.82	0.74	0.74	0.87	0.87	0.55
Acetonitrile	0.58	0.59	0.60	0.75	0.69	0.58
Ammonium	0.97	0.69	0.57	0.71	0.81	0.30
Benzene	0.79	0.76	0.78	0.92	0.88	0.66
BP	0.06	-0.12	-0.12	-0.07	-0.07	-0.07
C ₂ H ₄ O ₂ ⁺	0.69	0.81	0.85	0.97	0.85	0.74
C ₃ H ₈ O ⁺	0.60	0.83	0.98	0.81	0.83	0.51
C ₆ H ₁₀ O ⁺	0.47	0.79	0.98	0.73	0.76	0.48
Chloride	0.89	0.75	0.67	0.82	0.88	0.55
Naphthalene	0.64	0.66	0.70	0.94	0.78	0.81
Nitrate	0.95	0.73	0.57	0.72	0.81	0.30
NO	0.56	0.46	0.64	0.81	0.68	0.64
NO ₂	0.58	0.76	0.79	0.83	0.80	0.59
NO _x	0.60	0.60	0.74	0.87	0.76	0.66
O ₃	-0.43	-0.64	-0.66	-0.74	-0.64	-0.62
Ox	0.64	0.68	0.72	0.63	0.76	0.28
PAH	0.12	0.53	0.57	0.61	0.60	0.84
RH	0.87	0.52	0.49	0.72	0.70	0.41
SO ₂	0.15	0.65	0.49	0.58	0.51	0.65
Sulfate	0.98	0.54	0.48	0.60	0.72	0.18
Temperature	-0.24	-0.11	-0.13	-0.31	-0.14	-0.28
Toluene	0.70	0.77	0.84	0.88	0.88	0.64
WS	-0.33	-0.50	-0.48	-0.53	-0.50	-0.40

*We combined LO-OOA1 and LO-OOA2 into one factor LO-OOA.

Table S10. Detailed descriptions of the PMF solutions (CV-ACSM).

Factor Number	F _{peak}	Seed	Q/Q_{exp}	Solution Description
1	0	0	5.87	Too few factors and large residuals
2	0	0	3.56	Too few factors. Q/Q_{exp} substantially decreases (39% of the maximum Q) but there still exist large residuals at time periods and key m/z . One of the two factors is POA-like while another is OOA-like.
3	0	0	2.43	Too few factors. Q/Q_{exp} substantially decreases (19% of the maximum Q) but there still exist large residuals at time periods and key m/z . Two factors are POA-like and one is OOA-like.
4	0	0	1.75	Q/Q_{exp} still decreases very fast (12% of the maximum Q). The four factors are respectively CCOA-like, OOA-like, COA-like, and HOA-OOA mixed. More factors are needed.
5	0	0	1.46	Q/Q_{exp} decreases by 5% of the maximum Q . A new OOA factor is separated and therefore we identify two OOA factors, LO-OOA and MO-OOA. Except for LO-OOA, MO-OOA, and COA, the characteristic of the other three typical fossil-fuel-combustion factors (HOA, BBOA, and CCOA) are not clear, indicating certain mixing effects.
6	0	0	1.24	Optimum choices for PMF factors (MO-OOA, LO-OOA, HOA, COA, CCOA and BBOA). Time series and diurnal variations of PMF factors are consistent with the external tracers.
7-8	0	0	1.13- 1.05	Q/Q_{exp} decreases little (<2% of the maximum Q). Factors split, e.g., HOA and CCOA

Table S11. Correlation coefficients (Pearson's *R*) of the six OA factors determined by the CV UMR data with external tracers. The top-five values of each OA factor are bold.

	MO-OOA	LO-OOA	COA	BBOA	HOA	CCOA
Acetaldehyde	0.85	0.59	0.91	0.64	0.83	0.41
Acetone	0.88	0.58	0.86	0.60	0.82	0.42
Acetonitrile	0.62	0.41	0.64	0.51	0.70	0.47
Ammonium	0.97	0.59	0.78	0.48	0.63	0.20
Benzene	0.86	0.59	0.88	0.65	0.88	0.52
BP	0.04	-0.13	-0.07	0.03	-0.10	-0.12
C ₂ H ₄ O ₂ ⁺	0.76	0.65	0.88	0.68	0.91	0.59
C ₃ H ₈ O ⁺	0.68	0.67	0.95	0.59	0.77	0.37
C ₆ H ₁₀ O ⁺	0.56	0.65	0.90	0.54	0.72	0.35
Chloride	0.92	0.61	0.81	0.61	0.80	0.40
Naphthalene	0.73	0.50	0.77	0.66	0.91	0.69
Nitrate	0.94	0.64	0.77	0.47	0.62	0.20
NO	0.65	0.26	0.70	0.51	0.79	0.51
NO ₂	0.66	0.58	0.82	0.62	0.78	0.47
NO _x	0.70	0.38	0.79	0.58	0.84	0.53
O ₃	-0.48	-0.50	-0.66	-0.52	-0.72	-0.52
Ox	0.73	0.49	0.79	0.54	0.57	0.17
PAH	0.23	0.37	0.45	0.54	0.77	0.63
RH	0.89	0.46	0.70	0.49	0.67	0.28
SO ₂	0.19	0.56	0.39	0.49	0.60	0.58
Sulfate	0.97	0.45	0.72	0.39	0.52	0.10
Temperature	-0.24	-0.07	-0.18	-0.23	-0.21	-0.27
Toluene	0.78	0.58	0.89	0.67	0.86	0.48
WS	-0.36	-0.40	-0.49	-0.36	-0.51	-0.34

Table S12. The averaged uncertainties calculated for the PMF factors from the bootstrapping method (100 bootstrapping iterations for each dataset). The uncertainties are determined by the slope of linear regression of time-dependent standard deviation of the factor loadings from the bootstrapping analysis and the average factor loadings.

	CV, UMR	SV, HR	SV, UMR
LO-OOA	5%	17%	8%
MO-OOA	4%	7%	2%
COA	4%	12%	2%
HOA	6%	11%	5%
BBOA	5%	11%	5%
CCOA	6%	11%	2%

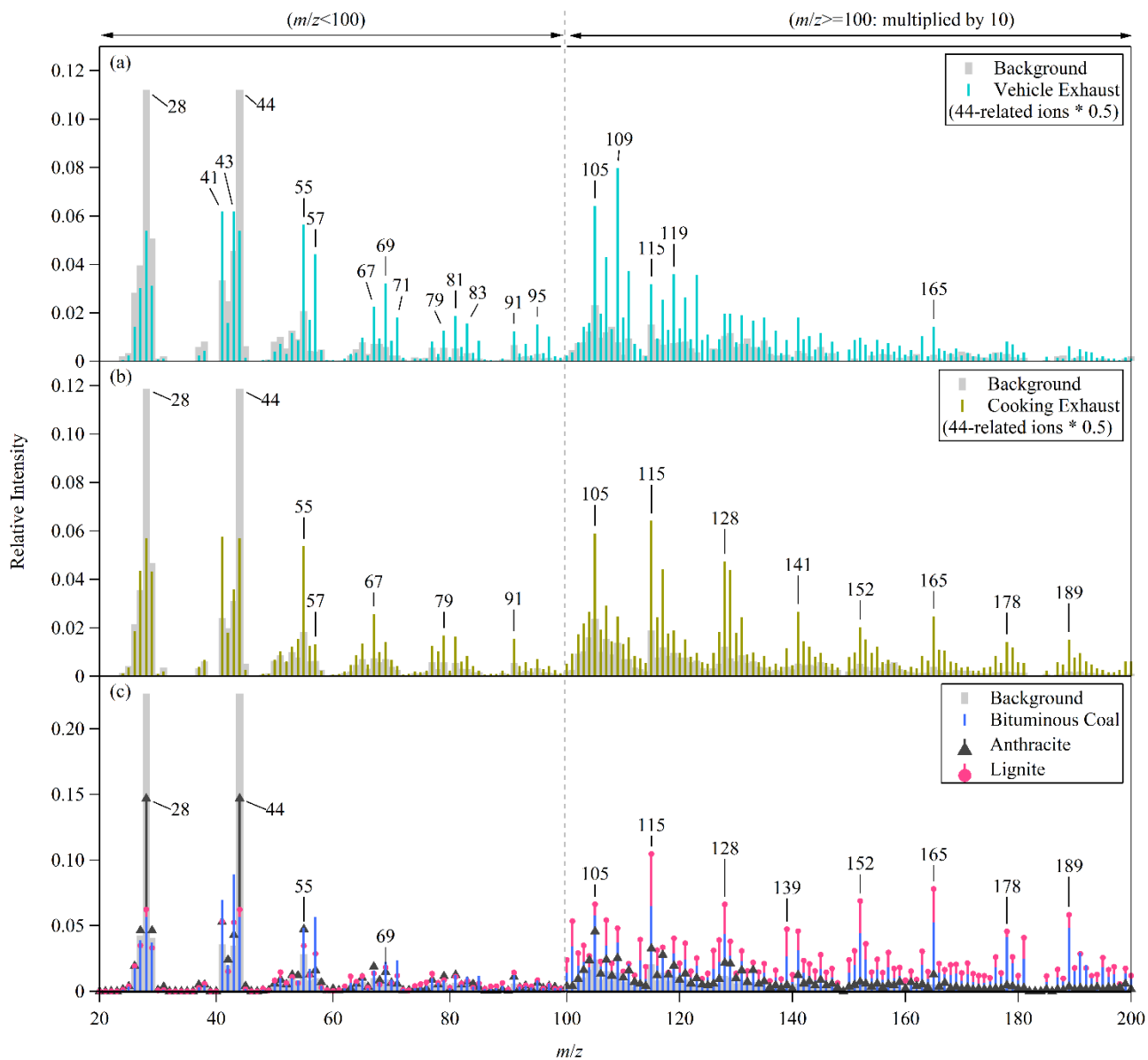


Figure S1. Comparisons of the CV-based OA mass spectra of (a) vehicle exhaust, (b) cooking plume, (c) WSOA from biomass burning, (d) coal combustion with the OA spectra of background air. In panels a and b, the 44-related ions (i.e., m/z 44, 28, 18) of all the mass spectra (including background) are multiplied by 0.5. For all panels, the intensity of the ions with $m/z > 100$ are multiplied by 10.

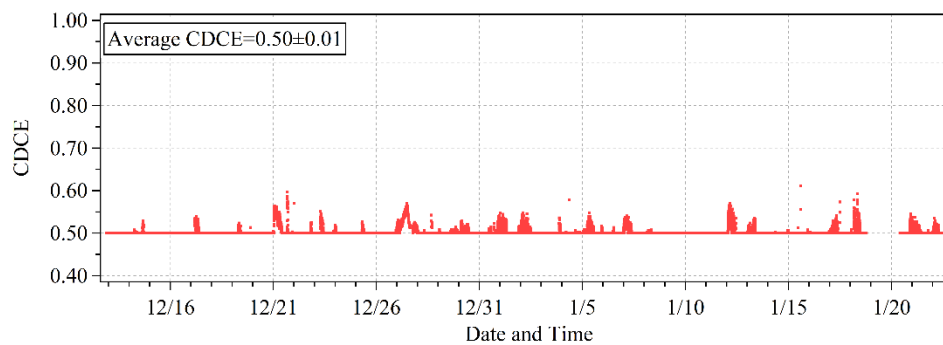


Figure S2. Time series of composition-dependent CE for the LTOF-AMS during the measurement period. These CDCE values are calculated based on the particle composition (Middlebrook et al., 2012).

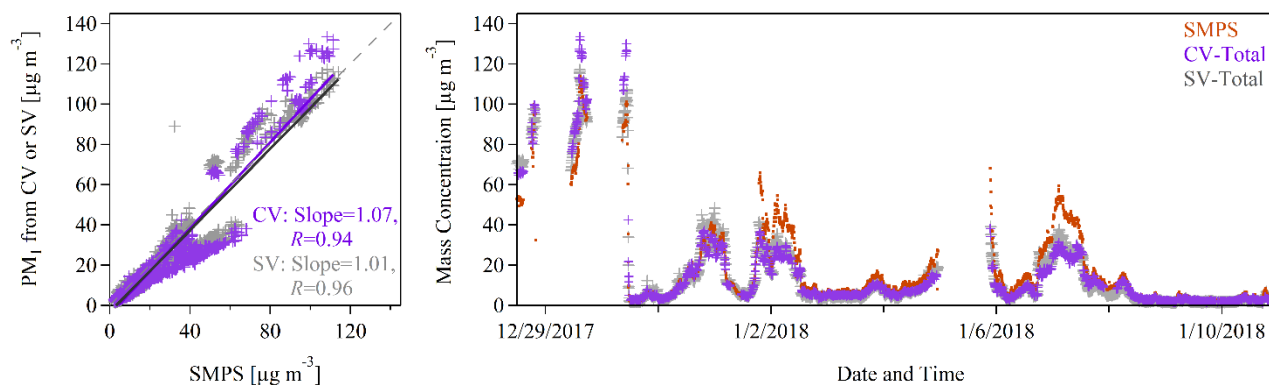


Figure S3. Scatter plot of the sum of the mass concentrations of NR-PM₁ and BC versus the PM₁ mass concentrations derived from the SMPS data. The number size distributions measured by the SMPS were converted to the mass size distributions and were then integrated to the mass concentrations by assuming spherical and non-porous particles. An estimated density of 1.35 g cm⁻³ based on the chemical composition (Hu et al., 2017) is used in this calculation. The concentrations of BC are derived from the measurements of the soot-particle (SP) mode of the LTOF-AMS by using the default CE of 0.5 and the RIE of 0.2 (Onasch et al., 2012).

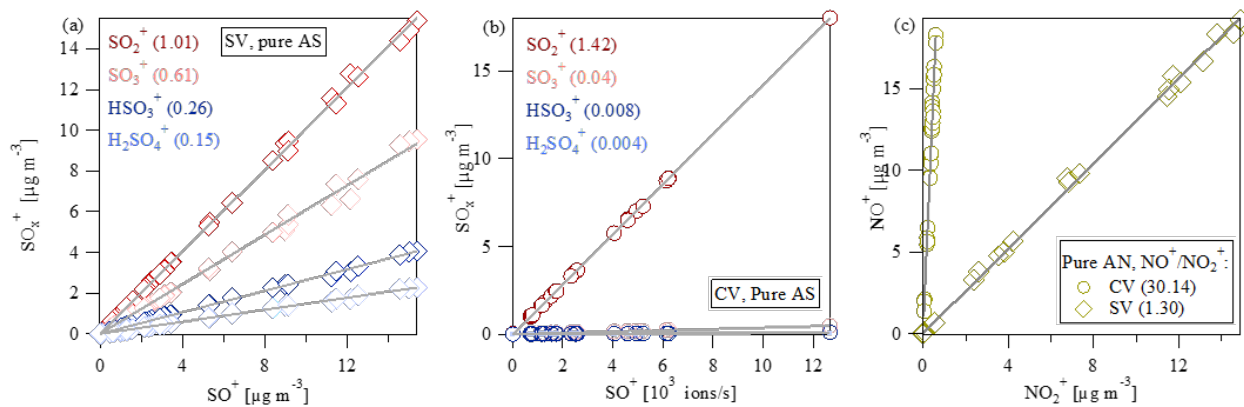


Figure S4. Scatter plots of (a) $\text{SO}_x^+/\text{SO}^+$ of pure $(\text{NH}_4)_2\text{SO}_4$ measured by SV-AMS, (b) $\text{SO}_x^+/\text{SO}^+$ of pure $(\text{NH}_4)_2\text{SO}_4$ measured by CV-ACSM (we assume that signals at 64, 80, 81, 98 are all contributed from the corresponding sulfate fragments of SO_2^+ , SO_3^+ , HSO_3^+ , H_2SO_4^+), (c) $\text{NO}^+/\text{NO}_2^+$ of pure NH_4NO_3 measured by both SV-AMS and CV-ACSM. The slopes of each regression line are listed in the parenthesis.

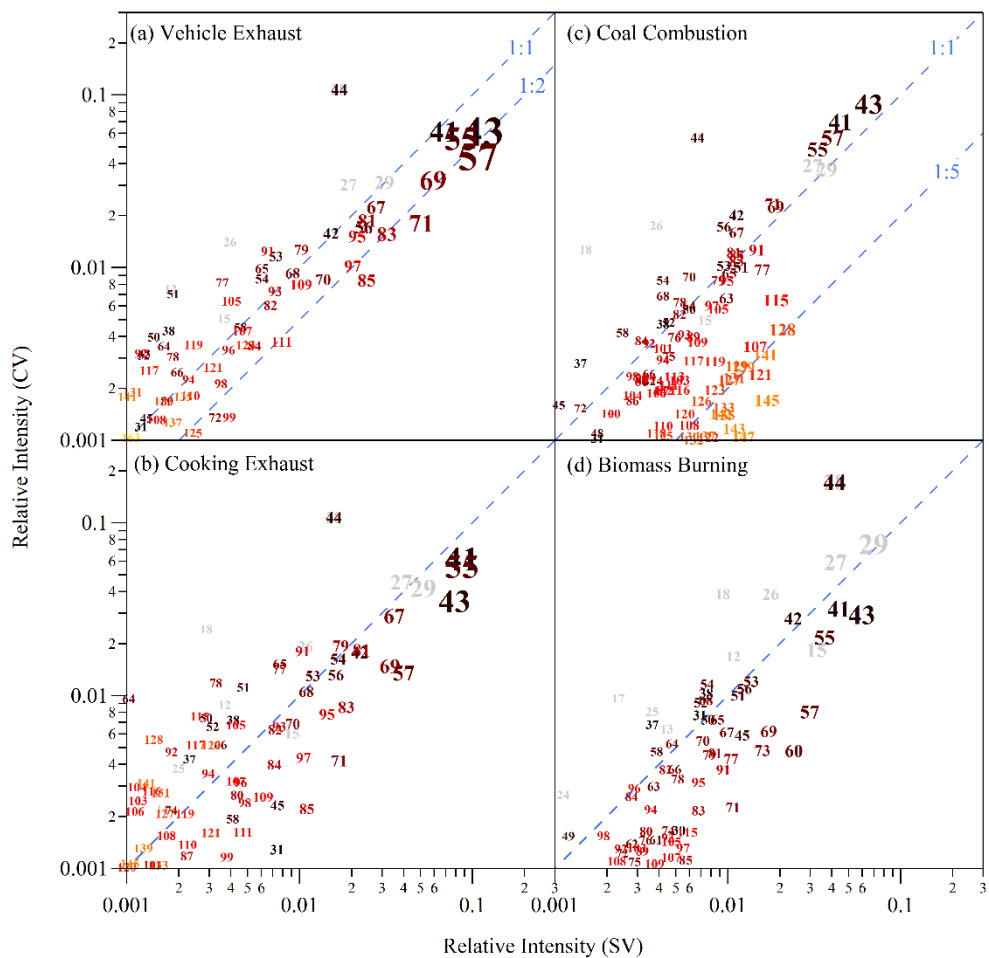


Figure S5. Scatter plot of the relative intensities of the ions in the CV and SV mass spectra from (a) vehicle exhaust, (b) cooking plume, (c) coal combustion, (d) biomass burning, all shown in Fig. 1. For vehicle exhaust, the SV spectra of gasoline car is used. For coal burning, the CV spectra of bituminous coal is used. For biomass burning, the CV spectra of rice straw is used in the scatter plot.

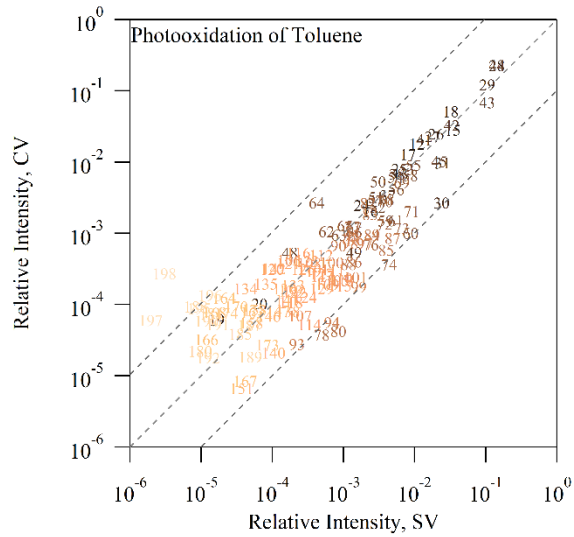


Figure S6. Scatter plot of the relative intensities of the ions in the CV and SV spectra of the SOA produced by the photooxidation of toluene.

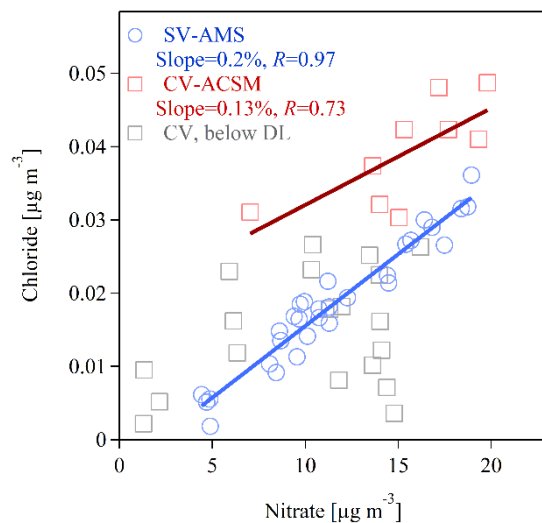


Figure S7. Scatter plot of nitrate and chloride mass concentrations detected by the CV TOF-ACSM and the SV AMS during IE calibrations on pure ammonium nitrate particles. The concentrations are shown as the nitrate equivalent mass concentrations. The data above the DL are used to perform the orthogonal distance regression with intercepts. The slopes and the correlation coefficients (Pearson's R) are shown in the legend.

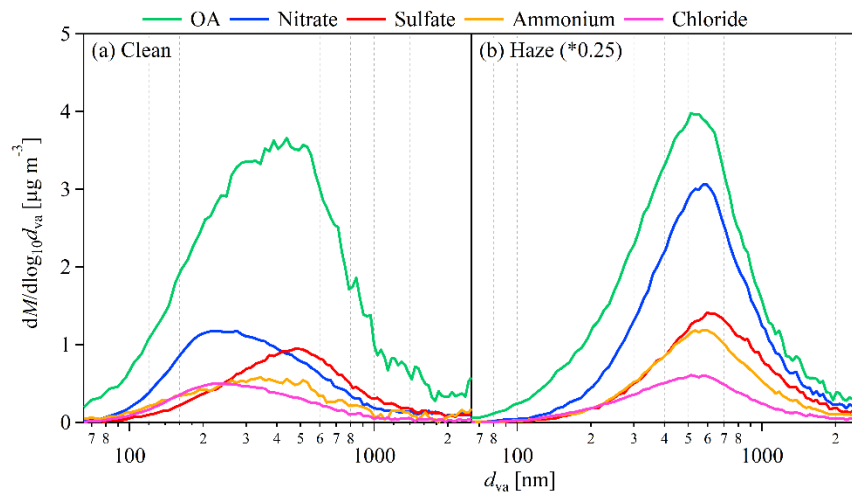


Figure S8. Averaged mass size distributions of OA, nitrate, sulfate, ammonium, and chloride during (a) clean and (b) haze periods in 2017 winter measured by the SV AMS.

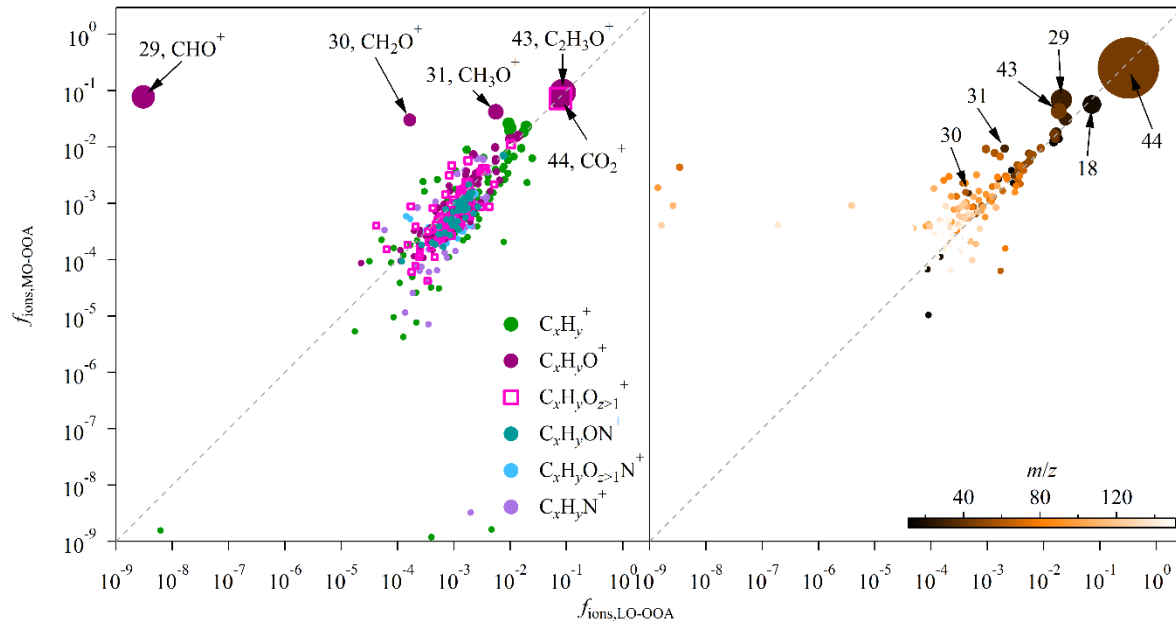


Figure S9. Scatter plots of the relative intensities of ions in the mass spectra of MO-OOA and LO-OOA, as determined by the PMF analysis on the SV and CV data. Markers in both panels are sized by the relative intensity with the same scale.

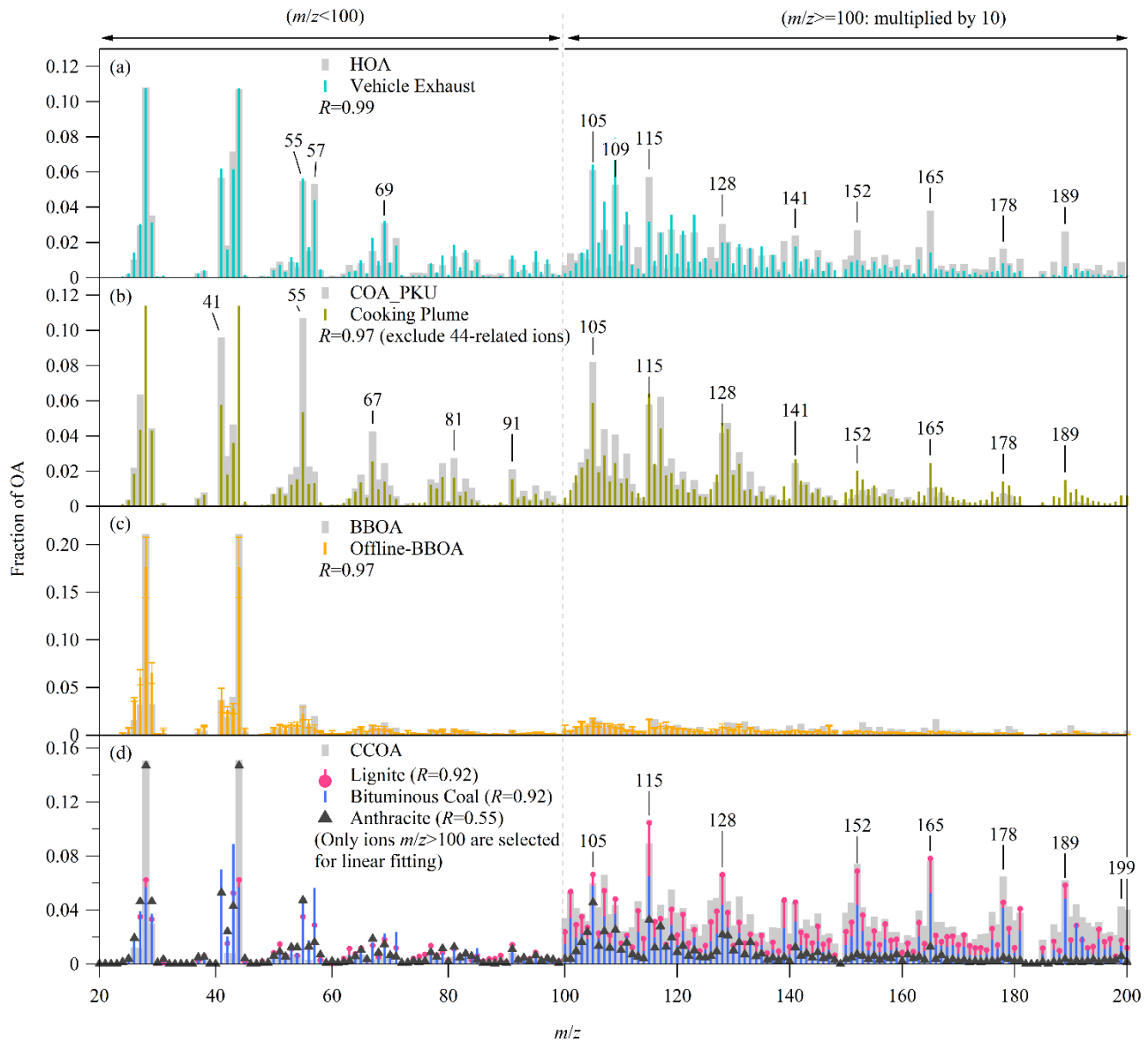


Figure S10. Comparisons of the mass spectra of four CV-based PMF factors with the spectra of specific primary OA described in Sect. 3.1.

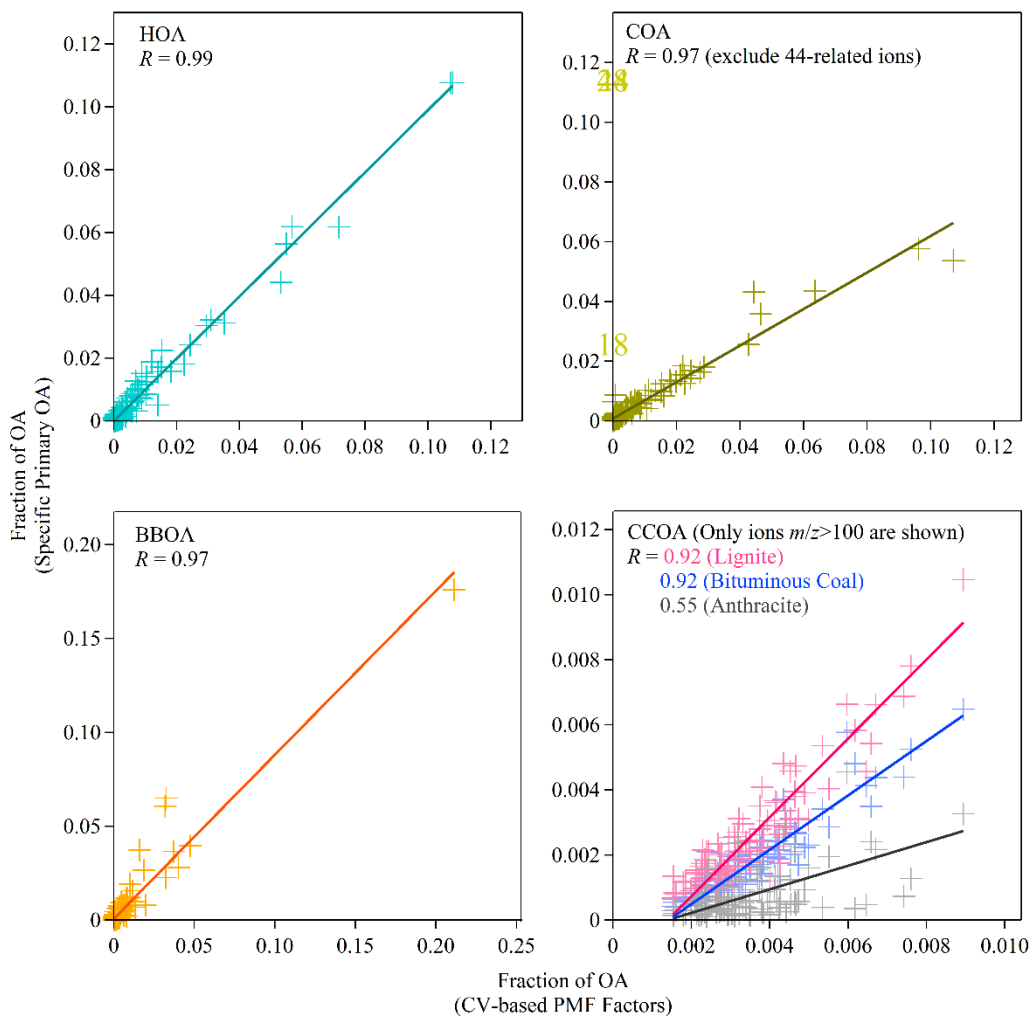


Figure S11. Scatter plots of the relative intensities of ions in the mass spectra of specific primary OA and the corresponding CV-based PMF factors.

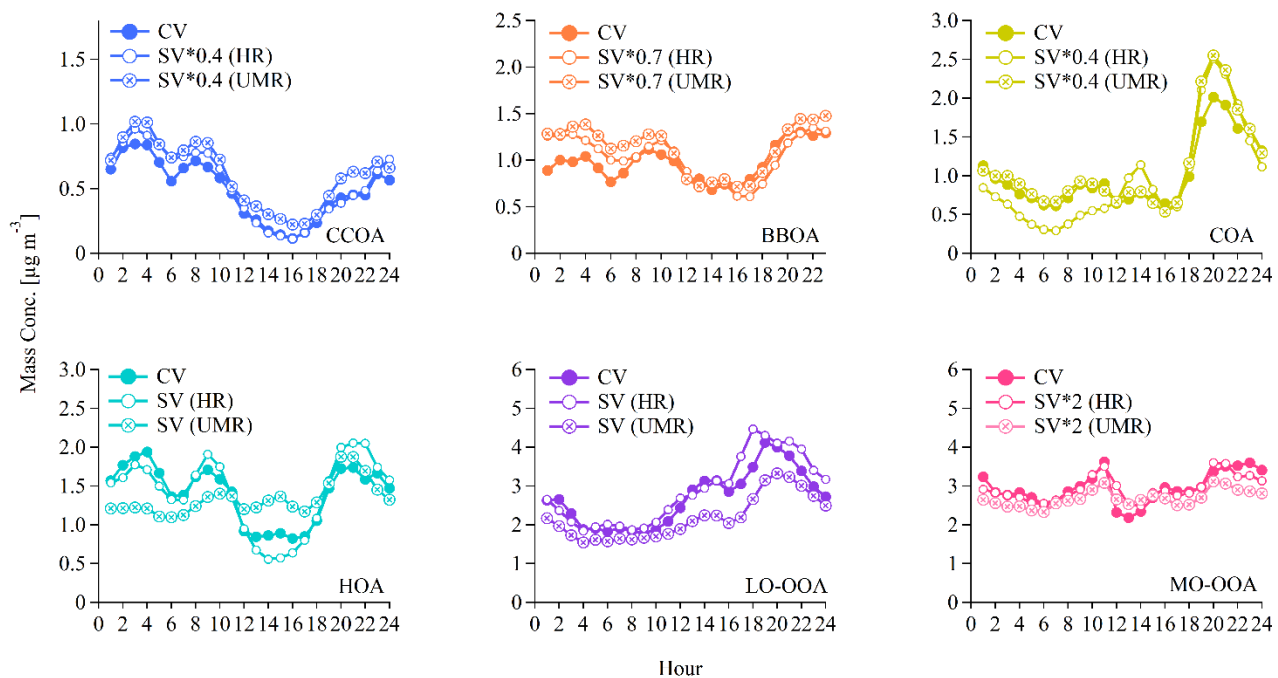


Figure S12. Diurnal patterns of the mass concentrations of each statistical PMF factors for the CV and SV data.

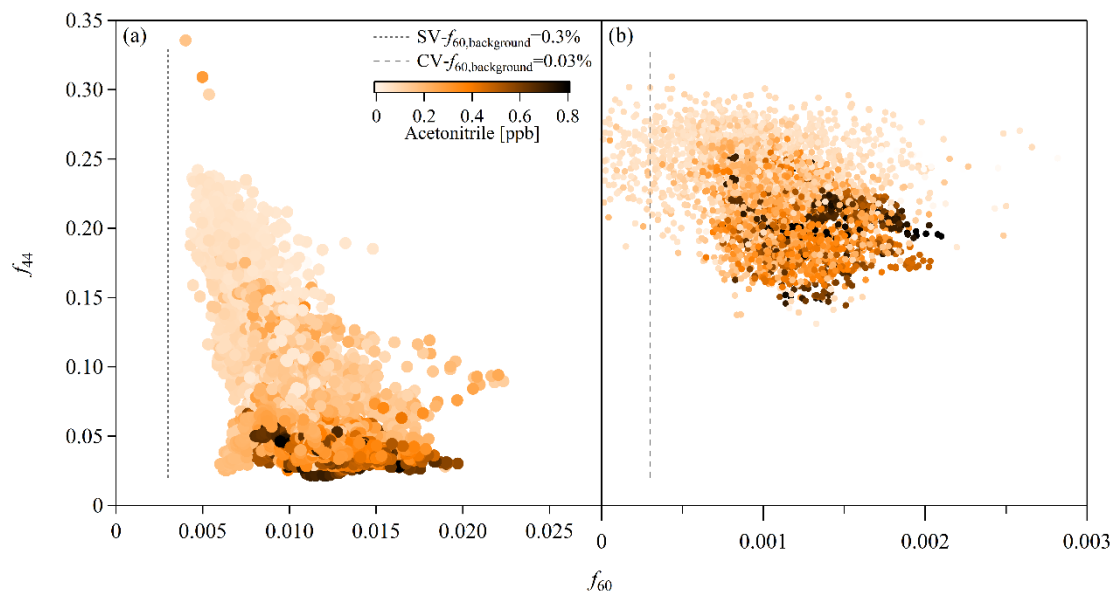


Figure S13. Scatter plots of f_{44} versus f_{60} in the (a) SV-AMS and (b) CV-ACSM spectra during the measurement period. The data are colored by the concentrations of acetonitrile. The vertical dashed line in panel (a) shows the background value of f_{60} for the SV data (Cubison et al., 2011) and the dashed in panel (b) shows the upper bound of the background value of f_{60} for the CV data.

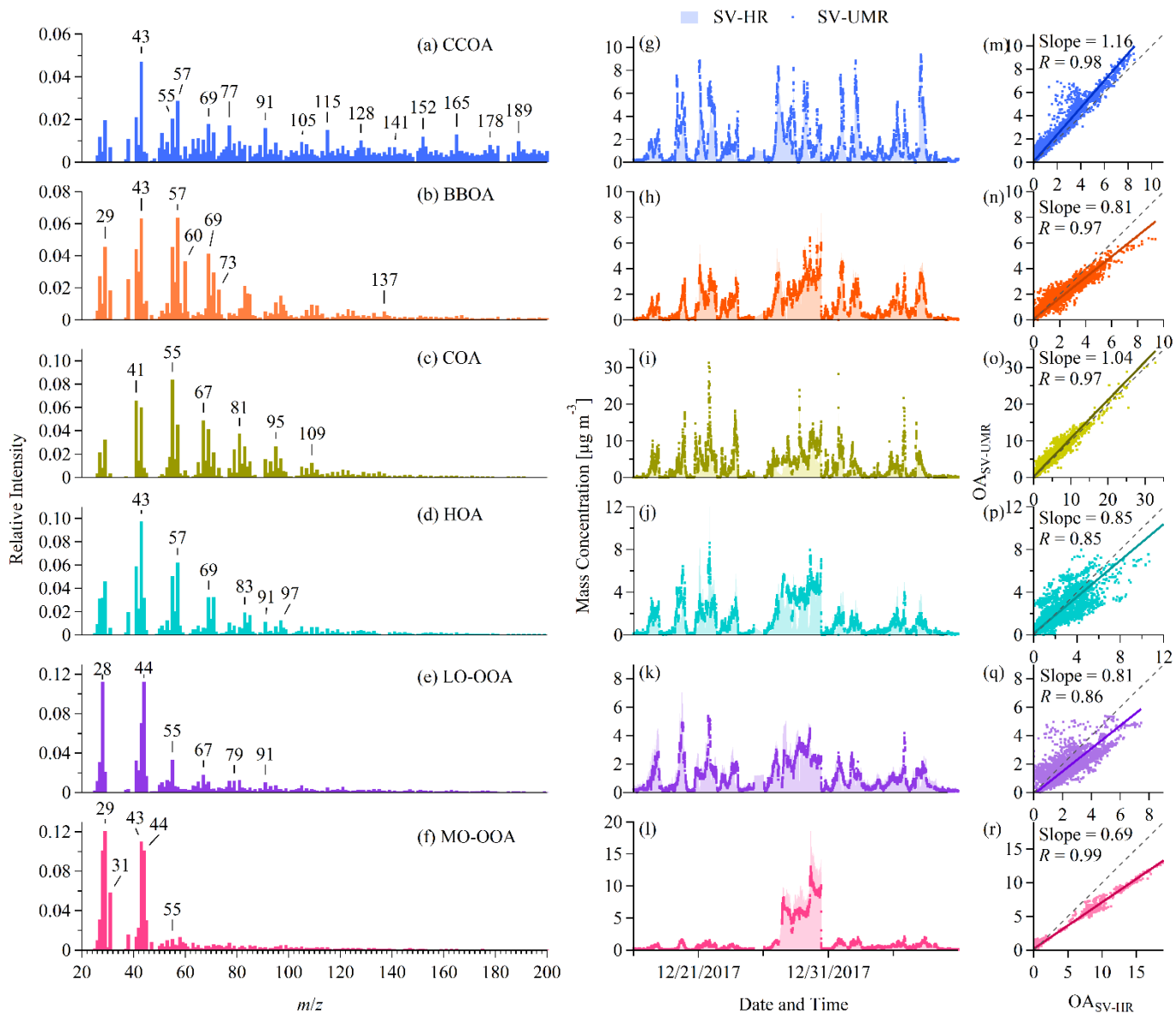


Figure S14. Comparisons of the UMR and HR PMF results from the SV AMS: (a-f) UMR mass spectra of the six OA factors, (g-l) time-series of the OA factors from both UMR and HR data, (m-r) scatter plots between the UMR factor and the corresponding HR factor. The thick lines in the scatter plots represent the orthogonal distance regressions with intercepts. The slopes and the Pearson's R values are shown in the legend.

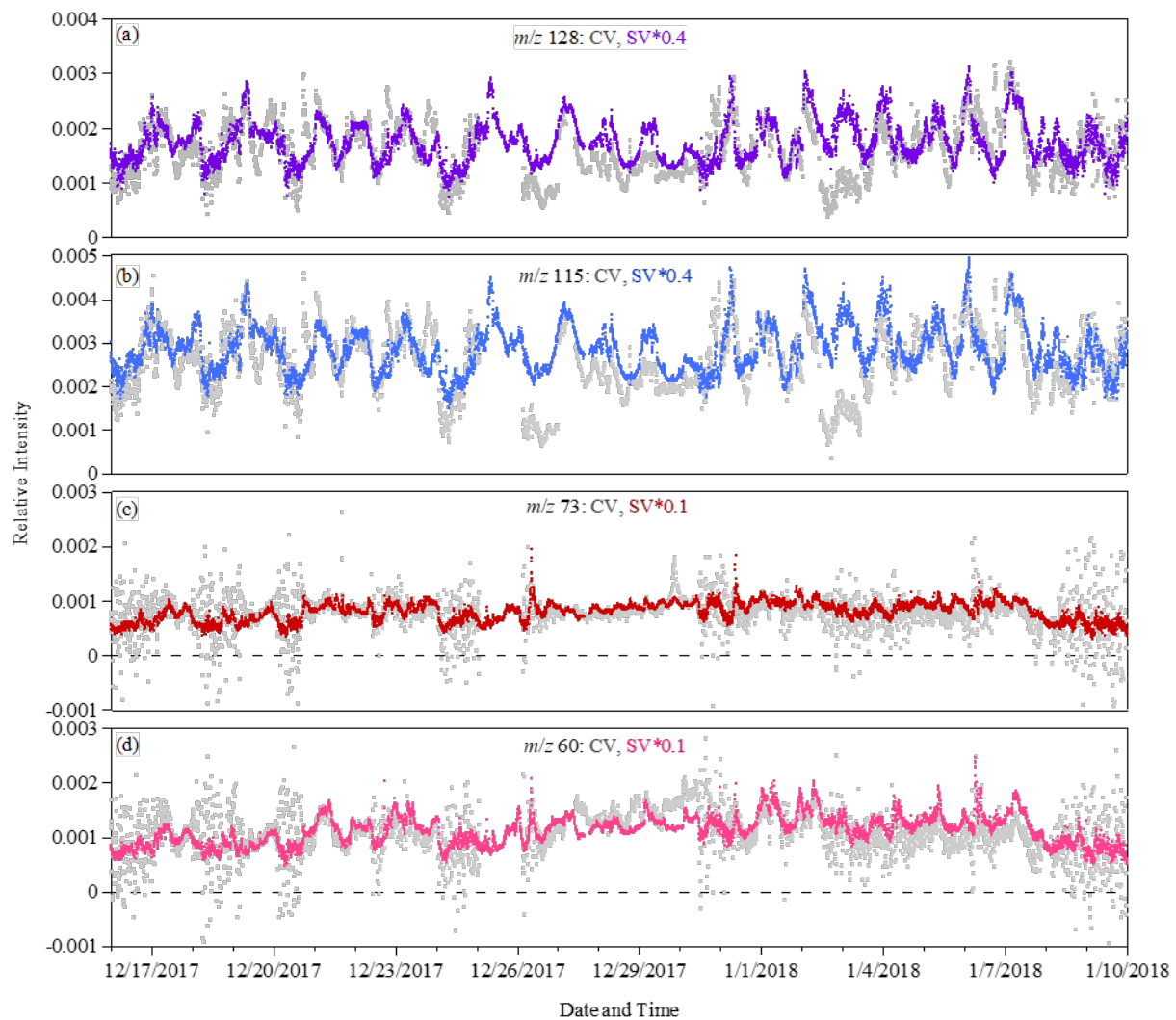


Figure S15. Comparisons of the relative intensities of m/z 128, 115, 73, 60 between the whole CV and SV spectra (not the spectra of PMF factors).

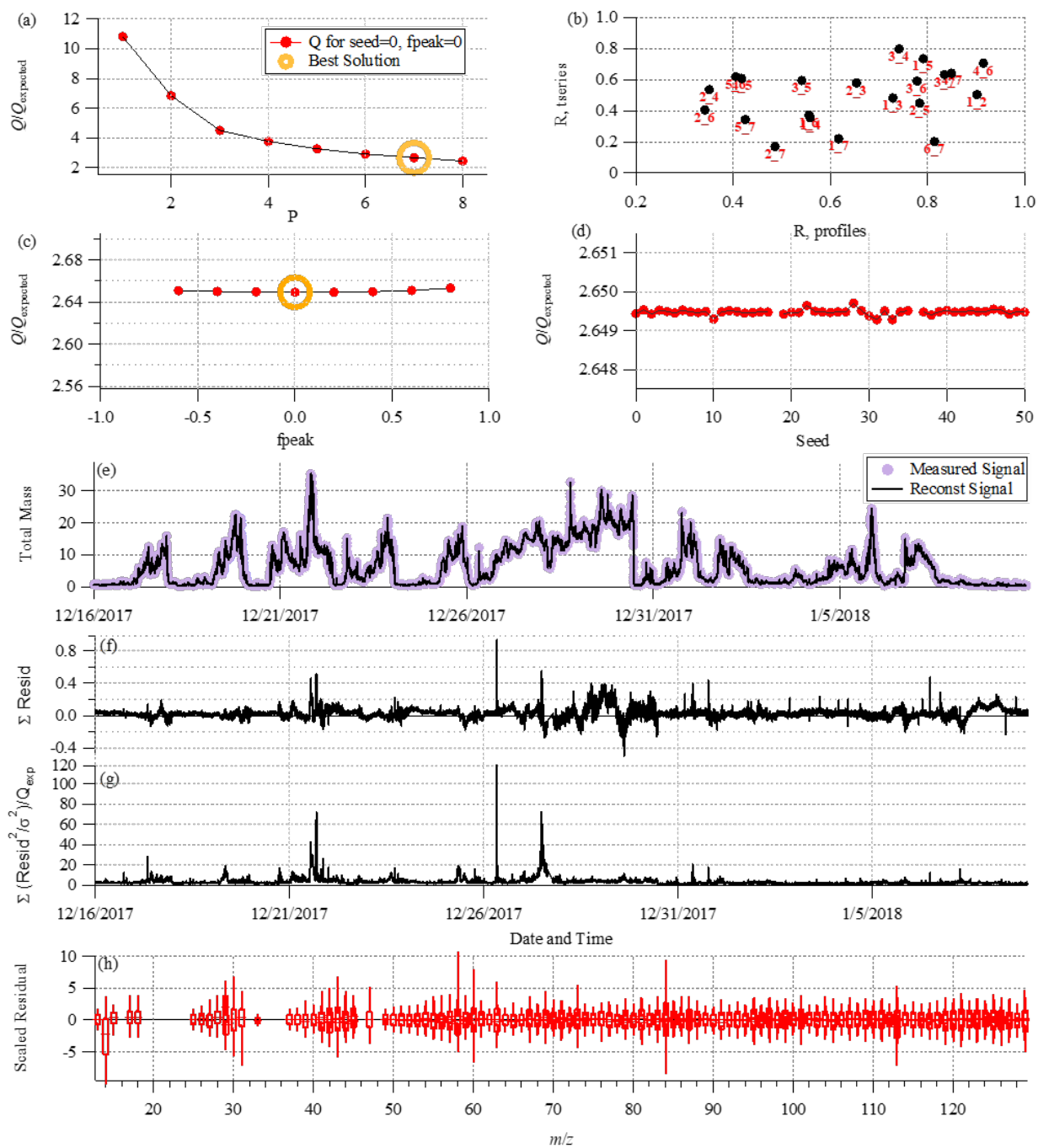


Figure S16. Diagnostics plots of the PMF analysis for the SV AMS (HR data).

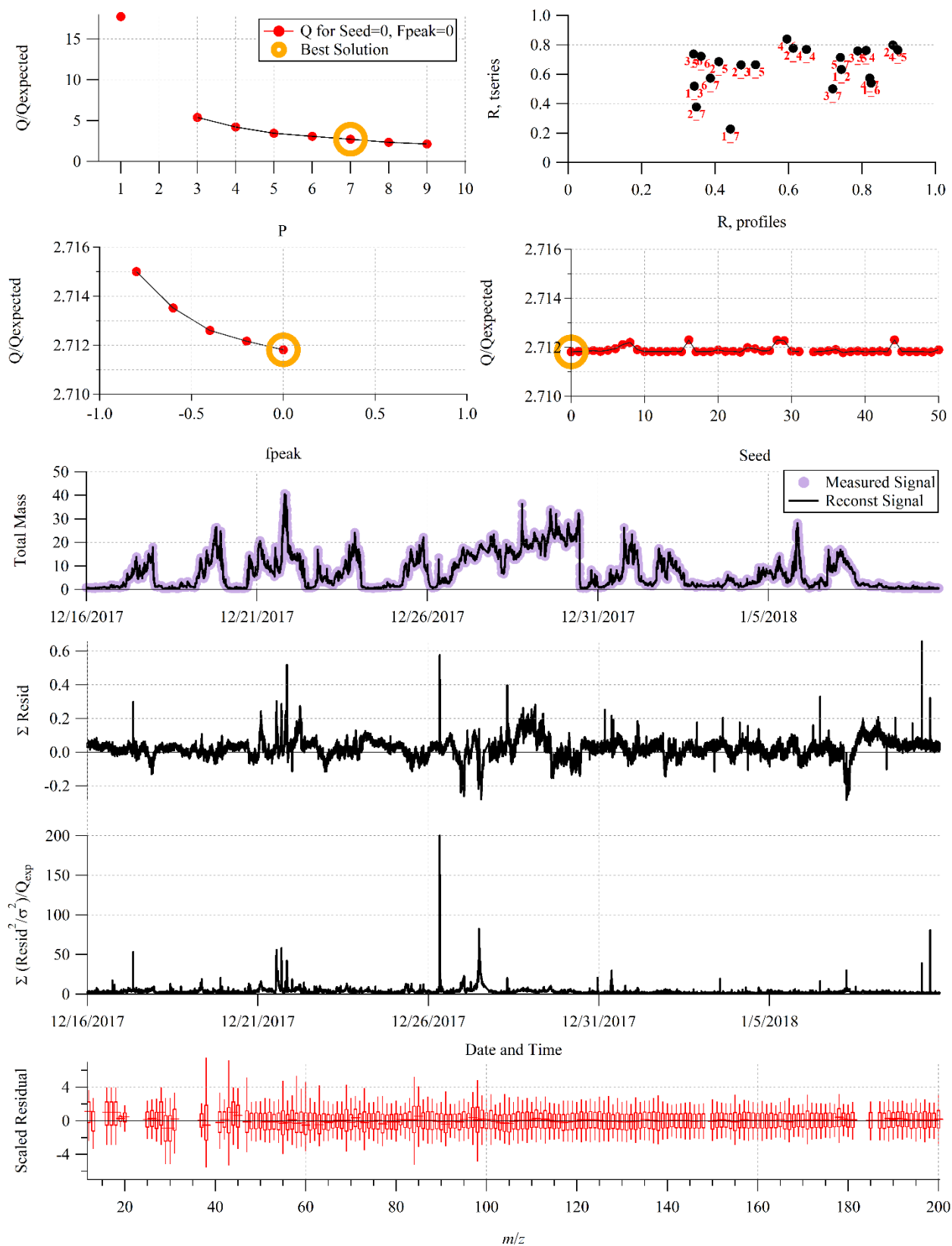


Figure S17. Diagnostics plots of the PMF analysis for the SV AMS (UMR data).

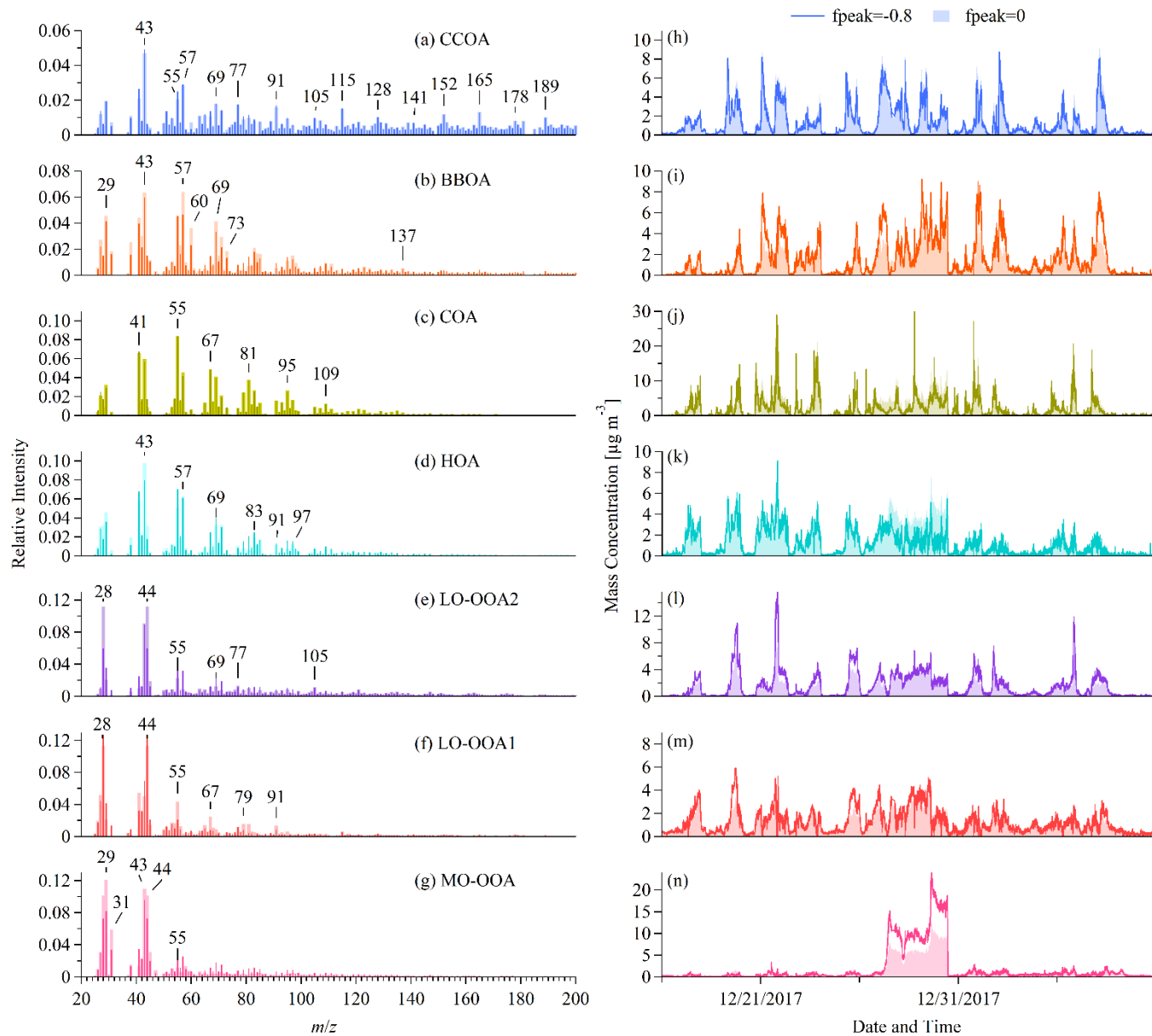


Figure S19. Comparisons of the time-series and the mass spectra of the seven OA factors at $f_{\text{peak}} = -0.8$ and 0 (SV-AMS, UMR).

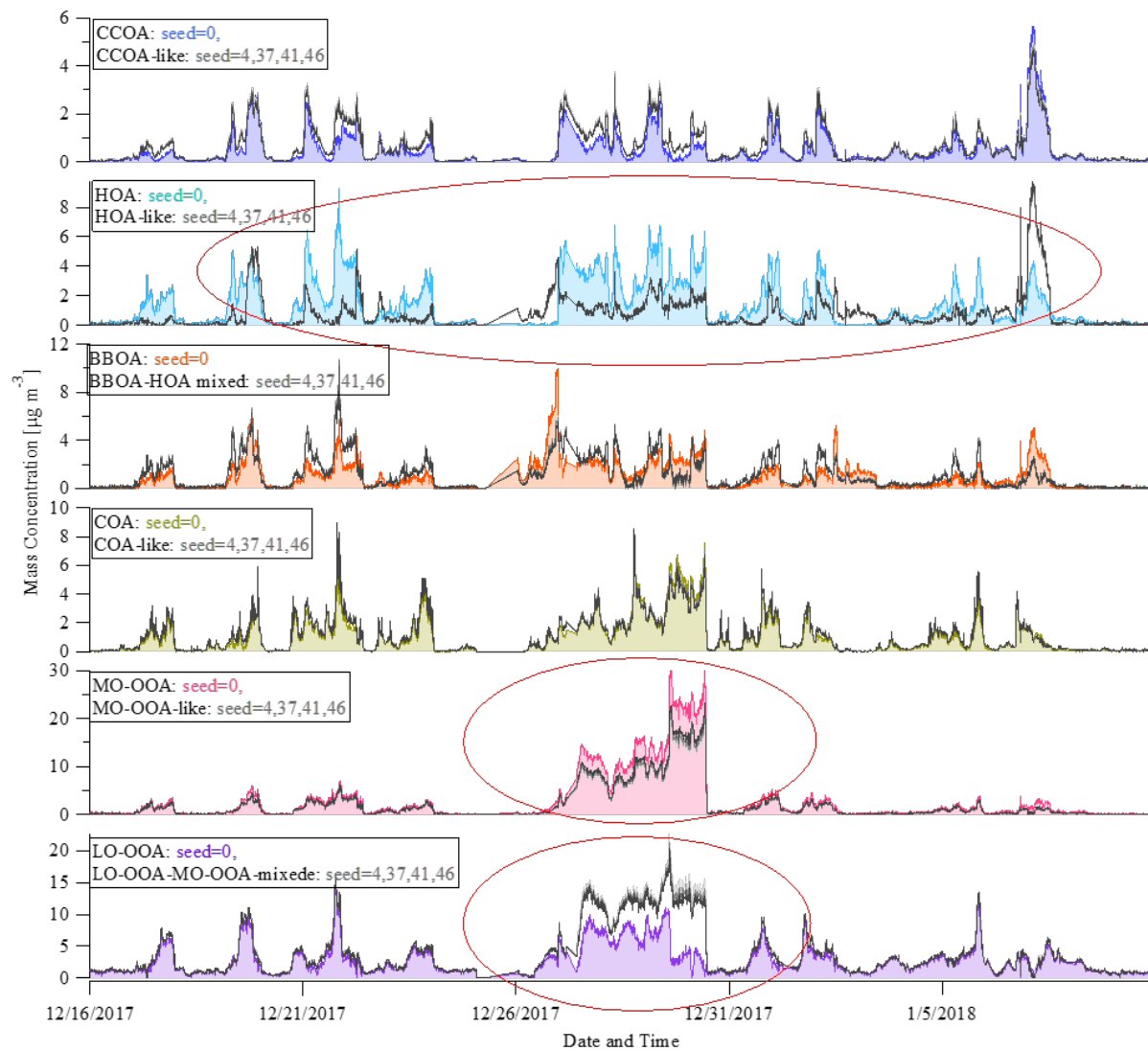


Figure S20. Comparisons of the time-series of the six OA factors at seed values of 0, 4, 37, 41, 46 for the PMF analysis of the CV-ACSM data.